

# Influence of Laser Cutting on the Functional Safety of Metallic Vascular Stents

György Meszlényi<sup>1</sup>, Enikő Bitay<sup>2,3</sup>

<sup>1</sup> Doctoral School on Safety and Security Sciences, Óbuda University, Népszínház str. 8., H-1081 Budapest, Hungary

<sup>2</sup> Department of Mechanical Engineering, Faculty of Technical and Human Sciences, Sapientia Hungarian University of Transylvania, Calea Sighişoarei nr. 2, 540485 Târgu-Mureş, Romania

<sup>3</sup> Bánki Donát Faculty of Mechanical and Safety Engineering, Óbuda University, Népszínház str. 8., H-1081 Budapest, Hungary

\* Corresponding author, e-mail: meszlenyi.gyorgy@uni-obuda.hu

Received: 02 February 2025, Accepted: 19 March 2025, Published online: 01 April 2025

## Abstract

A new method for the determination of missing data from scientific publications were presented on stent cutting lasers, using a combination of computational methods available from different sources in the literature. Some of the setting parameters for pulsed laser cutting are not independent of each other, which gives the possibility to determine some missing data in scientific articles: this way, data from different articles can be better evaluated, compared and experiments can be repeated, which is a useful basis for further development of a manufacturing technology. For this purpose, a new method was developed that allows the determination and calculation of the entire parameter system required for laser stent cutting. Finally, an evaluation system including weighting factors has been developed to quantify the defects of laser stent cutting, to classify the functional safety of the product, and to calculate the missing dimension that characterizes the cutting quality of stent manufacturing.

## Keywords

stent cutting lasers, parameters for pulsed laser cutting, defects of laser stent cutting

## 1 Introduction

### 1.1 New method for calculating the technological variables of stent manufacturing fiber lasers

Publications on fiber laser systems for producing vascular stents often do not provide all the technological variables needed to determine the important parameters of the focused beam's cross-section, the focal spot diameter and the Rayleigh length ( $Z_R$ ).

In fiber lasers, the resonator in the sealed box generates the laser radiation: laser diodes transfer their energy to an excitable optical fiber equipped with a Bragg grating [1] that act as an opening and closing mirror. From here, the beam is carried to the focusing head by the beam-transmitting optical fiber. The beam emerges from the beam-transmitting optical fiber in a spread pattern, which is parallelized by the collimating lens, and the parallel laser beam is concentrated on the workpiece by the focal lens.

The symbols described in Table 1 are the designation and units of quantities used in this article. In laser machining, the machining laser plays an important role, including the cross-sectional characteristic of the focused

beam, the focal spot diameter, because the focused beam is the tool that performs the machining by energy transfer. The formulas for the focal spot diameter – these are only valid for circular cross-section radiation beams – are generally the equivalent in the literature, but to achieve a common format, the focal spot radius may need to be doubled in some cases to obtain the focal spot diameter, and the beam quality data may need to be recalculated: if the beam spreading factor  $K$  is given, then its reciprocal, the beam quality factor  $M^2$ , is entered into Eq. (1) [2, 3]:

$$d_{f0} = \frac{4\lambda M^2 f}{d_b \pi}, \quad (1)$$

where  $\lambda$  is the wavelength of the laser radiation,  $f$  is the focal length of the lens focusing the laser beam on the workpiece,  $M^2$  is the beam quality factor, which tells us the multiplicity of the focal spot diameter of the beam under test compared to the beam following the ideal Gaussian distribution in the plane perpendicular to the beam propagation direction,  $d_b$  is the diameter of the near-parallel

**Table 1** Symbols, designation and units of quantities used

Symbol	Designation	Unit of quantity
$f$	Focal length of the focusing lens	mm
$f_{coll}$	Focal length of the collimating lens	mm
$d_{fc}$	Core diameter of the beam guiding optical fiber	$\mu\text{m}$
$d_b$	Diameter of the parallel laser beam	mm
$a_v$	Wall thickness of the tube	$\mu\text{m}$
$P_{av}$	Average power	W
$E_{v1}$	Energy per unit volume based on focal spot diameter	$\text{J}/\text{mm}^3$
$E_{v2}$	Energy per unit volume based on the cross-sectional width of the kerf	$\text{J}/\text{mm}^3$
$E_i$	Energy of one laser pulse	mJ
$d_{f0}$	Focal spot diameter	$\mu\text{m}$
$\lambda$	Wavelength	$\mu\text{m}$
$D_{BT}$	Distance between two pulses	$\mu\text{m}$
$f_i$	Pulse frequency	kHz
$P_i$	Pulse power	W
$t_i$	Pulse duration	ms
$M^2$	Beam propagation factor $M^2$ (dimension-less)	
$Z_R$	Rayleigh length	$\mu\text{m}$
PO	Spot overlap (dimension-less)	
$k_1$	Kerf cross section width on top	$\mu\text{m}$
$k_2$	Kerf cross section width on bottom	$\mu\text{m}$
$v$	Cutting speed	mm/s

laser beam in front of the focal lens, the number  $\pi$  is a mathematical constant, approximately equal to 3.14, it is the ratio of a circle's circumference to its diameter. From Eq. (1) for the spot diameter of a focused laser beam, it follows that the smaller the value of the  $M^2$  factor, the smaller the area over which the beam energy can be focused [4].

Definition of  $Z_R$ : stigmatic beams: distance in the direction of propagation from the respective beam waist for which the beam diameter or the beam width are equal to  $\sqrt{2}$  times their respective values at the beam waist [5]. Therefore the pulse energy per unit area is half that calculated in the focal spot. Usually, a beam is in focus within twice the  $Z_R$ , so twice the  $Z_R$  is called the focal depth. Equation (2) is very similar to the spot diameter formula, except that the focal length of the focusing lens and the diameter of the beam in front of the lens are squared [2].

$$Z_R = \frac{4\lambda M^2 f^2}{d_b^2 \pi} \quad (2)$$

What also justifies this analysis is that in laser machining, the part of the beam close to the focal spot is used, is only important: where the focus is, what the focal spot

diameter and the twice  $Z_R$  are within which the laser can work. What are the additional benefits of testing the two quantities above? Based on these two variables, the geometry of the focused beam can be described by functions: the beam diameter as a function of the  $z$  coordinate in the direction of beam spreading, where  $Z_0$  is the  $z$  coordinate of the focal plane [2].

There is also a formula in the scientific literature for the focused laser beam's focal spot diameter, of fiber laser where  $f$  is the focal length of the lens focusing the laser beam on the workpiece,  $d_{fc}$  is the core diameter of the beam guiding optical fiber,  $f_{coll}$  is the focal length of the collimator paralleling the beam: this is summarized by Eq. (3) [6, 7]. Equation (3) is called an approximate formula in both literatures cited, so the values calculated from it are given for two valuable digits.

$$d_{f0} = \frac{d_{fc} f}{f_{coll}} \quad (3)$$

The optical elements discussed so far, and the laser beam path are shown in Fig. 1. Analyzing Eq. (1), if the focal length of the focusing lens is decreased, then in principle the spot size decreases linearly, and it follows from Eq. (2) that the  $Z_R$  decreases quadratically. Analyzing Eq. (1), if the laser beam is expanded by a factor of  $x$ ,

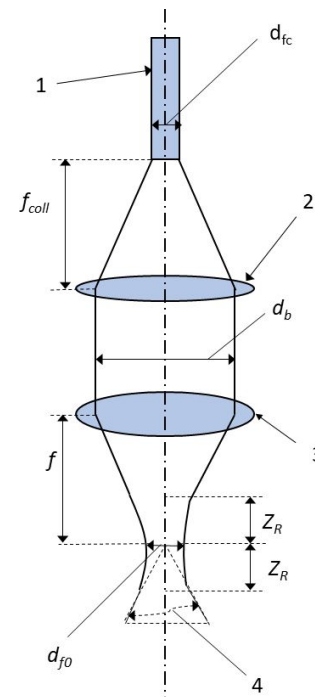


**Fig. 1** Illustration of the main characteristics of a focused laser beam. 1: transporting fiber core, 2: collimator, 3: focusing lens, 4: divergence angle,  $d_{fc}$ : core diameter of the beam guiding optical fiber,  $d_b$ : diameter of the parallel laser beam,  $f$ : focal length of the focusing lens,  $Z_R$ : Rayleigh length,  $d_{f0}$ : focal spot diameter

then in principle the spot size decreases as a function of  $1/x$ , and from Eq. (2) it follows that the  $Z_R$  decreases as a function of  $1/x^2$ . In principle, because using a shorter focal length focusing lens increases spherical aberration, the beam spreading coefficient is reduced, so  $d_{f0}$  and  $Z_R$  are not so strongly reduced [4].

Where do these factors come in? The smaller the spot size, the more concentrated the energy, so higher machining speeds can be achieved, but because the  $Z_R$  is smaller, only thinner materials can be machined. When cutting tubes, one of the applications of which is the cutting of expanding stents, the wall thickness is small anyway (~0.100 mm), so a small spot size can be used, and in this case the advantage of the small  $Z_R$  is that the beam will be defocused on the internal tube wall opposite the machining, and thus spread out, so that there will be little or no thermal transformation in the opposite inner tube wall (Fig. 2).

A rational use of the units and the precision of the calculated and measured quantities shown in this paper:

- One point of reference is the use of reasonable units of measurement used in literature. The usual measurement unit of  $df_0$  in Eq. (1) is  $\mu\text{m}$ , so it is also worth substituting  $\lambda$  on the other side of Eq. (1) in  $\mu\text{m}$ , while  $f$  is usually given in mm, so it is worth to substitute  $db$  in that unit as well. The other thing to note is that Eq. (3) is an approximation, so the data calculated from it, including the focal length, is enough to provide two significant digits.
- The other difficulty is that many of the characteristics

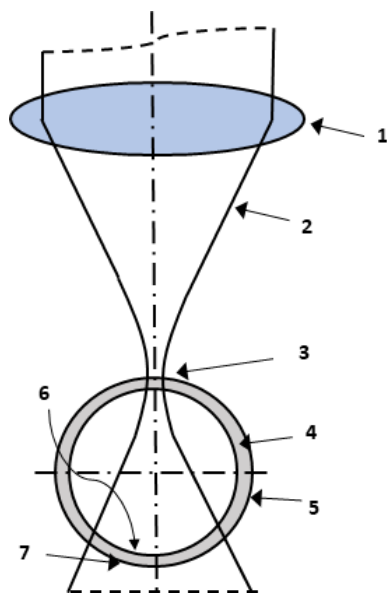


**Fig. 2** Longitudinal section of a focused laser beam when cutting a tube; 1: focusing lens, 2: vertical cross section of focused laser beam, 3: cut side, 4: cross section, 5: outer wall / outer side, 6: internal side, 7: external side

in this paper vary over wide ranges, which implies that the calculated characteristics vary over wide ranges: at the beginning of the paper, there were laser devices with milliseconds pulse duration, then ns and fs pulse durations, the later ones having a high pulse frequency, so giving some characteristics of these lasers in normal form is necessary.

Table 2, which gives the accuracy of the calculated and measured quantities presented in this article, has been prepared according to the above criteria and will be used as a basis for Eq. (4):

$$d_b = \frac{4\lambda M^2 f}{d_{f0}\pi} \tag{4}$$

Chen et al. [8] show the input data in their article from which the diameter of the parallel laser beam can be calculated first by rearranging Eq. (1), which gives Eq. (4). The diameter of the parallel laser beam after inserting the data from the first column of Table 3 is 3.8 mm, so all the data is now available to calculate the  $Z_R$ , which is  $96 \mu\text{m}$  according to Eq. (2).

In Demir et al. [9] with important input data is shown, by substituting it in column 2 of Table 3, all the data are available to calculate the focal length of the focusing lens, for which by rearranging Eq. (1), it leads to Eq. (5), which yields 60 mm. All the data are then available to calculate the  $Z_R$ , which results in  $230 \mu\text{m}$  according to Eq. (2).

$$f = \frac{d_{f0}d_b\pi}{4\lambda M^2} \tag{5}$$

**Table 2** The accuracy of the quantities calculated or measured

Symbol	Unit of measurement	Calculated or measured accuracy
$f$	mm	Rounded to tenths of mm
$d_{fc}$	$\mu\text{m}$	Rounded to $\mu\text{m}$
$d_b$	mm	Rounded to tenths of mm
$P_{av}$	W	Rounded to tenths of W
$E_{v1}$	$\text{J}/\text{mm}^3$	Rounded to $\text{J}/\text{mm}^3$ or normal form
$E_{v2}$	$\text{J}/\text{mm}^3$	Rounded to $\text{J}/\text{mm}^3$ or normal form
$E_i$	mJ	Rounded to the hundredth mJ
$D_{BT}$	$\mu\text{m}$	Rounded to hundredth of a $\mu\text{m}$ or normal shape
$f_i$	kHz; Hz	Rounded to Hz
$P_i$	W	Rounded to W or normal form
$Z_R$	$\mu\text{m}$	Rounded to $\mu\text{m}$
PO		Rounded to the hundredths of a percent
$k_1$	$\mu\text{m}$	Rounded to $\mu\text{m}$
$k_2$	$\mu\text{m}$	Rounded to $\mu\text{m}$

**Table 3** Beam characteristics of stent cutting fiber lasers\*

Beam characteristics	Publication			
	Chen et al. [8]	Demir et al. [9]	García-López et al. [10]	Catalano et al. [11]
$d_{f0}$ (μm)	12	23	20.8	23
$d_{fc}$ (μm)	–	–	50	–
$f$ (mm)	30	60	50	60
$f_{coll}$ (mm)	–	–	120	–
Wavelength (μm)	1.07	1.064	1.07	1.064
$M^2$ beam propagation ratio	1.1	1.7	2.82	1.7
$d_b$ (mm)	3.8	5.9	9.2	6.0
$Z_R$ (μm)	96	230	113	230

\* The calculated missing data are in italic

In García-López et al. [10], from which the diameter of the beam-guiding fiber can be calculated, by using the data in column 3 of Table 3 [8–11] expressing  $d_{fc}$  from Eq. (3), this gives 50 μm, then from Eq. (4) the diameter of the parallel beam is calculated to be 9.2 mm, then the  $Z_R$  is calculated from Eq. (2) to give 113 μm.

Finally, extracting data from Catalano et al. [11], the diameter of the parallel laser beam can be calculated by substituting the data from column 4 of Table 3 into Eq. (4), which is given by 6.0 mm. The ZR can then be calculated in the usual way, obtaining 230 μm. The IPG YLP-1/100/50/50 Q-coupled fiber laser used by Catalano et al. [11] differs from the one used in previous articles in that it can emit pulses of up to 100 ns.

The laser systems used in the experiments analyzed so far, as well as the characteristics and geometries of the materials used, are listed in Table 4 [8–11].

Comparing the range of some of the important data of the stent-cutting lasers considered in this paper with those of the micromachining fiber lasers considered in

Meszlényi and Bitay [4] (Table 5), the following conclusions can be drawn:

- the average focal spot diameter of stent-cutting lasers is smaller, allowing higher energy concentration and higher cutting speeds;
- the average focal length of the focusing lens of stent-cutting lasers is smaller, resulting in a smaller focal length (see Eq. (1));
- the average focal length of the collimator lens of stent-cutting lasers is larger, resulting in a smaller focal diameter (see Eq. (3));
- the average  $Z_R$  of stent-cutting lasers is smaller, which still allows the tube wall to be cut through but helps to defocus the laser beam focused on the opposite inner wall of the tube (Fig. 2).

Here is a method presented to determine the missing data of stent fiber lasers in scientific publications, using a combination of formulas found in different places in the literature.

**Table 4** Tested lasers and machining data

Cutting conditions	Publication			
	Chen et al. [8]	Demir et al. [9]	García-López et al. [10]	Catalano et al. [11]
Laser manufacturer, type	–	MedPro fiber laser workstation from PRECO Company	MedPro fiber laser workstation from PRECO Company	IPGYLP-1/100/50/50 Q-switched fiber laser
Material	316LVM	AZ31 magnesium alloy	AISI 316L stainless steel	AISI 316L stainless steel
Tube wall thickness (μm)	80	200	220	200
Tube diameter (mm)	3.0	2.5	3.0	–

**Table 5** Comparison of stent cutting and general micro-machining laser data

	Stent-cutting lasers studied in this article	Commonly used micromachining fiber lasers [4]
$d_{f0}$ (μm)	12–23	9.4–73
$f$ (mm)	30–80	50–190
$f_{coll}$ (mm)	50–120	28.4–50
$Z_R$ (μm)	96–367	131–3154

## 2 Method for calculating missing technological variables in laser cutting

The setup parameters for laser cutting with a pulsed laser are not independent of each other, which gives the possibility to calculate some missing data of articles: this way, data from different articles can be better compared and experiments can be repeated, which is a useful basis for further development of a technology. The data system for laser machining is given in Table 1.

These simple formulas are listed in Eqs. (6) to (10):

$$P_{av}(\text{W}) = E_i(\text{mJ})f_i(\text{kHz}). \quad (6)$$

The average power is equal to the product of the pulse energy and the pulse frequency, here the millijoule unit would be divided by 1000 and the kHz unit would be multiplied by 1000, these are simplified Eq. (6):

$$v(\text{mm/s}) = D_{BT}(\mu\text{m})f_i(\text{kHz}). \quad (7)$$

Now let's define the distance between two pulses ( $D_{BT}$ ): the distance between the centers of two successive pulses hitting the workpiece.

The cutting speed is the product of the distance between two pulses on the material and the pulse frequency. Here, due to the  $\mu\text{m}$  unit of measurement, there would be a division by 1000 to convert to mm, and a multiplication by 1000 due to kHz, these would be simplified Eq. (7):

$$P_i(\text{W}) = \frac{E_i(\text{mJ})}{t_i(\text{ms})}. \quad (8)$$

Pulse power is the ratio of the pulse energy to the pulse duration. Here the milli prefixes are dropped.

Calculating the energy per unit volume using the focal spot diameter:

- Dividing 1000  $\mu\text{m}$  by the distance between two pulses, which is expressed in  $\mu\text{m}$ , gives the number of pulses per 1 mm of cut length, multiplying this by the energy of one pulse, leads to the energy per 1 mm of cut length. Now the calculation of the volume in which this energy is distributed is needed. The volume is obtained by multiplying the length of 1 mm by the cross-section, which in this case is the wall thickness multiplied by the focal spot diameter. Here the milli prefix is simplified since the energy is in millijoules, the material thickness in microns must be converted in millimeters with a division by 1000.  $d_{f0}$  is in microns, it must be converted in millimeters with a division by 1000. This calculation assumes that the average width of the kerf is the same as

the width of the focal spot, so it underestimates the melted volume, which the Eq. (9) divide by it gives a higher energy per unit volume. To obtain a result that can be easily evaluated, the measurement unit of energy per unit volume is now  $\text{J}/\text{mm}^3$  (Eq. (9)):

$$E_{v1} = \frac{E_i 1000 \mu\text{m}}{D_{BT} 1 \text{ mm } a_v \left( \frac{d_{f0}}{1000} \right)}. \quad (9)$$

Calculating the energy per unit volume by the width of the cut-off gap:

- Dividing 1000  $\mu\text{m}$  by the distance between two pulses gives the number of shots per 1 mm of cut length, multiplying this by the energy of a pulse, leads the energy per 1 mm of cut length. Now the calculation of the volume in which this energy is distributed is needed. The volume is obtained by multiplying the length of 1 mm by the cross-section, which in this case is the wall thickness multiplied by the upper width of the cross-section of the cut kerf. This method of calculation assumes that the average width of the cross-section of the kerf is the same as the width of the top of the kerf, but the cross-section of the kerf is usually conical, so the bottom of the kerf is smaller than the top, and so Eq. (10). overestimating the volume melted, by which it is dividing, and so it gives less energy per unit volume. To obtain a result that can be easily evaluated, the unit of energy per unit volume is now  $\text{J}/\text{mm}^3$ :

$$E_{v2} = \frac{E_i 1000 \mu\text{m}}{D_{BT} 1 \text{ mm } a_v \left( \frac{k_1}{1000} \right)}. \quad (10)$$

Two approaches to estimating energy per unit volume are used because not all the data are given in the literature, some giving only the focal spot diameter, others only the width of the kerf, some both.

These analyses neglect the energy absorbed in the plasma stream, which does not get into the material, and the energy lost through the cut-off gap and other heat conduction and radiation.

## 3 Definition and formula of spot overlap

The impact of pulsed laser cutting on materials is characterized by some important technological parameters: the pulse energy, the pulse duration, the distance between two pulses due to the combined effect of the cutting speed and the pulse frequency, and the two interpretations of

the energy per unit volume, which were described earlier. It is also important how large the diameter of the cut spot is: this is the basis for calculating the spot overlap, the smaller the spot overlap, the closer the pulses fired onto the material are to each other.

In practice, the spot created as an intersection of the laser beam and the workpiece is replaced by a better measurable focal spot diameter given in articles or in the laser equipment specification.

From Muhammad's PhD thesis [1], it follows that the author uses the term pulse overlap for the previously used cut spot overlap, which means the overlap of the cut spots along the linear coordinate, of two consecutive pulses (Fig. 3). This is to be understood as if the laser pulses in one place, then the spot overlap is 100%, and if the circumference of one spot passes through the center of the next, then there is 50% overlap. This shows that it is not a spatial overlap, but an overlap along the x-coordinate of the cut direction. If the spots touch each other, there is 0% overlap. The pulse overlap is incorrect because the pulse is a three-dimensional body that interacts with the material being machined in a time-varying manner.

Muhammad's (pulse overlap) formula [1], Eq. (11) is the like in the article of Thawari et al. [12]:

$$PO = \left( 1 - \frac{v}{d_{f0} f_i} \right) \quad (11)$$

The spot overlap formula of Thawari et al. [12] is shown in Eq. (12):

$$d_{f0} (1 - PO) f_i = v \quad (12)$$

Our own formula includes the distance between two pulses, which based on Eq. (7) corresponds to Eq. (13), where the second form of Eq. (13) is the more meaningful percentage of spot overlap:

$$PO = 1 - \frac{D_{BT}}{d_{f0}} \quad \text{or} \quad PO = \left( 1 - \frac{D_{BT}}{d_{f0}} \right) \times 100\% \quad (13)$$

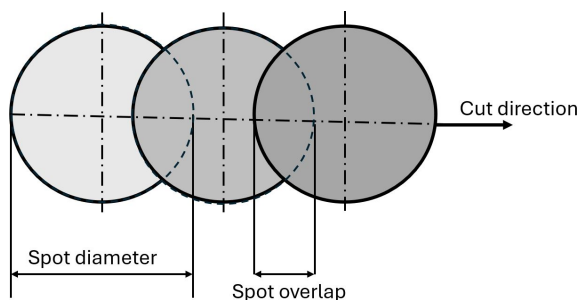


Fig. 3 Illustration of the spot overlap

It follows from the similarity of the formulas that all three terms mean the same thing, but since the reference is the diameter of the spot, it is best to call it spot overlap. Fig. 4 shows the spot overlap in practice.

Now let's analyze the effect of the change of spot overlap on the cutting speed:

- The pulse frequency limits the cutting speed: if there is no spot overlap on the material, only discrete holes are formed, or bridges are formed due to a small change in pulse energy (Fig. 4 (a)). If there is no spot overlap, then the theoretically achievable cut speed can be calculated, for example if the pulse frequency is 1500 Hz and the focal spot size is 0.024 mm: the maximum achievable cut speed is:  $1500 \text{ s}^{-1} \cdot 0.024 \text{ mm} = 36 \text{ mm/s}$  which does not cause a cut.
- The actual achievable cutting speed is half of this (50% overlap) = 18 mm/s (Fig. 4 (b)). In a previous experiment of us, the maximum cutting speed was around this: 15 mm/s was achieved [13].
- This line of thought is only true if an impulse can penetrate matter. However, it has been shown in experiments that at higher frequency and lower energy combinations, a pulse does not drill through the material, so the achievable cutting speed is lower [13], and ultrashort pulse (ps, fs) pulse cutting causes a thin layer of material to evaporate, so ablation is the way to cut the material, and a spot overlap of over 90% is required [1, 14].
- If the spot overlap is 100%, the laser is firing in one place and there is no cut.

#### 4 Analysis of Nd:YAG laser stent cutting data in the scientific literature to the end of the chapter

Calculation of missing data from Kathuria [15] for the second setting: according to Eq. (8), dividing the pulse energy of 80 mJ by the pulse duration of 0.1 ms gives

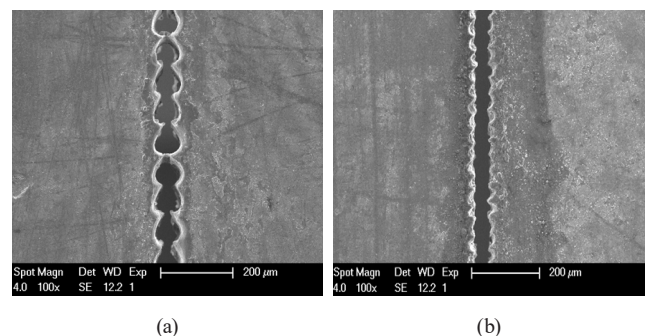


Fig. 4 Spot overlap from experiments; (a) No spot overlap: unreliable cut: bridges are formed; (b) Cutting spot overlap of around 50% enables fast cutting

a pulse power of 800 W. Then, solving Eq. (7) for  $D_{BT}$ , dividing the cutting speed by the frequency gives a distance between two pulses of 5.57  $\mu\text{m}$ . However, in the article by Kathuria [15], at the first setting the pulse energy is less than a tenth, while the pulse duration is half, so that only 130 Watts of pulse power is obtained, and the distance between two pulses is 1.17  $\mu\text{m}$  given the high pulse frequency of 1 kHz. The calculated values are shown in italics in Table 6. In these articles, the size of the focal spot is not given, nor is the width of the kerf, so the calculation of the energy per unit volume is not possible. In these articles the laser cut stent is made of 316L material.

The machining of the last 3 columns in Table 6 were performed with the Nd:YAG laser used at the Department of Materials Science and Technology of BME, the variation of the focal spot diameter of this laser was analyzed in a previous paper and came out to 24  $\mu\text{m}$  [16] at a beam expander setting of 8, which was used for cutting stents to achieve small focal spot diameter and small  $Z_R$ . Thus, for these machining operations, the energy per unit volume can be calculated based on the laser spot diameter by substituting the data into Eq. (9), and the results are shown in the penultimate row of Table 6. From Eq. (13), the spot overlap for the last 3 machining operations can be calculated and is above 85 %. This is explained by the fact that pulse energies of 3 mJ and below were used, and if 1 pulse cannot penetrate the material, then a larger overlap is required, based on our previous analysis.

Bitay et al. [17] show cutting of 316LVM material, while in the last two experiments they used nitinol. The pulse energy is calculated by rearranging Eq. (7) equals 2.67 mJ, the pulse power is then calculated from Eq. (8) to be 1.335 W.

In Nagy and Dobránszky [18], let's first look at setting 1: the average power is given by Eq. (6) as 9.6 W, and Eq. (8) gives a pulse power of 160 W. by dividing the pulse energy of 2.4 mJ by the pulse duration of 0.015 ms. Then, using Eq. (7) for DBT, dividing the cutting speed by the frequency gives a distance between two pulses of 2.5  $\mu\text{m}$ .

In Nagy and Dobránszky [18], let's now look at setting 2: the average power from Eq. (6) is 9 W, and from Eq. (8), dividing the pulse energy of 3 mJ by the pulse duration of 0.02 ms, leads a pulse power of 150 W. Then, using Eq. (7) for DBT, dividing the cutting speed by the frequency gives a distance between two pulses of 3.3  $\mu\text{m}$ .

Analyzing Table 6 row by row, shows that a higher average power is needed to cut nitinol, which is achieved by increasing the pulse frequency to 4 kHz and 3 kHz, respectively, according to Eq. (6). The energy per unit volume of the three last articles [17, 18] was the highest: 506 J/mm<sup>3</sup>, due to the small firing distance caused by the low cutting velocity Eq. (9).

An analysis of data from publications in the scientific literature on Nd:YAG laser stent cutting with sufficient data for additional calculations is now presented. The calculation missing data from Eqs. (6) to (13) so that the experiments can be repeated. The new data calculated are shown in italics in Table 6 [15, 17, 18].

**Table 6** Calculated missing data for Nd:YAG laser stent fabrication\*

	Unit of measurement	Kathuria [15]	Kathuria [15]	Bitay et al. [17]	Nagy and Dobránszky [18]	Nagy and Dobránszky [18]
Material		316L	316L	316LVM	Nitinol	Nitinol
Wall thickness	$\mu\text{m}$	100	100	110	100	100
Average power	W	6.5	2.4	4.0	9.6	9.0
Pulse time	ms	0.05	0.1	0.002	0.015	0.02
Pulse energy	mJ	6.5	80	2.67	2.4	3
Pulse power	W	130	800	1335	160	150
Pulse frequency	Hz	1000	30	1500	4000	3000
Cutting speed	mm/s	1.17	0.17	3	10	10
Distance between two pulses on material	$\mu\text{m}$	1.17	5.57	2	2.50	3.33
Focal spot diameter	$\mu\text{m}$	–	–	24.00	24.00	24.00
Spot overlap	%	–	–	91.67	89.58	86.11
Energy per unit volume based on focal spot diameter	J/mm <sup>3</sup>	–	–	506	400	375
$Z_R$	$\mu\text{m}$	–	–	60	60	60

\* The calculated missing data are in italics

**5 Analysis of Nd:YAG laser stent cutting data**

Let's analyze the data from Meszlényi and Izápy [13]. According to Eq. (8), the division of the pulse energy of 8 mJ by the pulse duration of 0.02 ms, gives a pulse power of 400 W. The laser settings were the same in the experiments, only the cutting speed was varied, so the distance between two pulses row in Table 7 [13] can be calculated from Eq. (7), the spot overlap from Eq. (13), for the volumetric energy input only the focal spot diameter was given, so it can only be calculated from Eq. (9), the  $Z_R$  was estimated in Meszlényi and Bitay [16]. Table 7 shows the calculated new data in italics.

Analyzing the data in Table 7, it is obvious that the maximum achievable cutting speed of 15 mm/s is the technological optimum, with the smallest spot overlap and the largest distance between two pulses, and the lowest adherent slag formation due to the minimum energy per unit volume. Such high cutting speeds are not found in the analyzed literature for pulsed Nd:YAG laser stent cuts. The outer casing of the tube cut during this experiment is shown in Fig. 5, while the slag formation on the inner side is shown in Fig. 6. The material was 304L stainless steel tube with a wall thickness of 120  $\mu\text{m}$ .

**6 Analysis of fiber laser stent cutting data from the literature**

The calculated missing data for stent production with fiber laser, are given in italics in Table 8 [8, 11, 19–22].  $Z_R$ s are taken from Table 3, as described there. Using the data given in Chen et al. [22], the  $Z_R$  for his experiment can be calculated and is found to be 160  $\mu\text{m}$ .

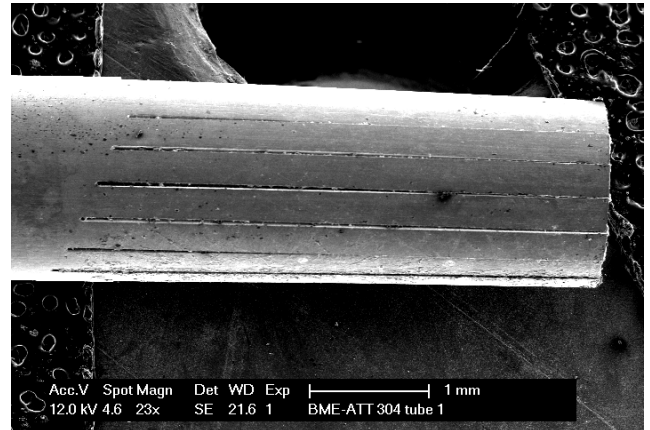


**Fig. 5** Cuts on the outer surface of the tube are made with a 1500 Hz pulse frequency. The cutting speed increases from 2.5 to 40 mm/s along the direction of the cut from the top to the bottom of the figure. At higher cutting speed the cuts were not successful

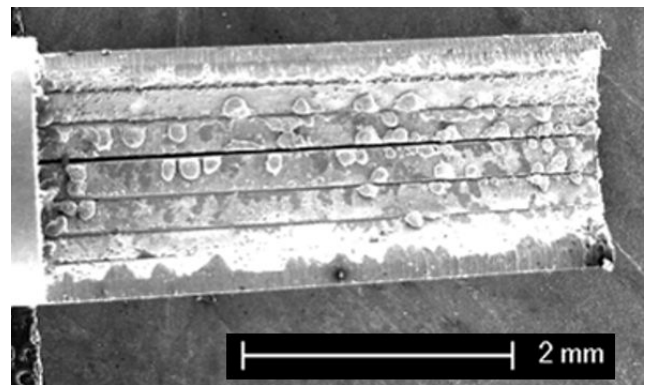


**Fig. 6** Cuts on the outer surface of the tube are made with a 1500 Hz pulse frequency. The cutting speed increases from 2.5 to 40 mm/s along the direction of the cut from the top to the bottom of the figure. At higher cutting speed the cuts were not successful

**Table 7** Experiment data with varying cutting speed\*

Material	Unit of measurement	Meszlényi and Izápy [13]					
		1	2	3	4	5	6
Wall thickness	$\mu\text{m}$	120	120	120	120	120	120
Average power	W	12	12	12	12	12	12
Pulse time	ms	0.02	0.02	0.02	0.02	0.02	0.02
Pulse energy	mJ	8	8	8	8	8	8
Pulse power	W	<i>400</i>	<i>400</i>	<i>400</i>	<i>400</i>	<i>400</i>	<i>400</i>
Pulse frequency	Hz	1500	1500	1500	1500	1500	1500
Cutting speed	mm/s	1.5	3	4.5	6	9	15
Distance between two pulses on material	$\mu\text{m}$	<i>1.00</i>	<i>2.00</i>	<i>3.00</i>	<i>4.00</i>	<i>6.00</i>	<i>10.00</i>
Spot overlap	%	<i>95.83</i>	<i>91.67</i>	<i>87.50</i>	<i>83.33</i>	<i>75.00</i>	<i>58.33</i>
Energy per unit volume based on focal spot diameter	$\text{J}/\text{mm}^3$	<i>2778</i>	<i>1389</i>	<i>926</i>	<i>694</i>	<i>463</i>	<i>278</i>
$Z_R$	$\mu\text{m}$	<i>60</i>	<i>60</i>	<i>60</i>	<i>60</i>	<i>60</i>	<i>60</i>

\* The computed data are in italics

Kleine et al. [19] show an ideal laser setting, it was taken as the basis. The average power is given by Eq. (6) as 1.5 W, and Eq. (8) gives a pulse energy of 3.00 mJ if the pulse power of 30 W is multiplied by the pulse duration of 0.1 ms.

According to Eq. (6) by Meng et al. [20], if the average power of 7.0 W is divided by the pulse frequency of 1.5 kHz, then a pulse power of 4.67 mJ is obtained, then according to Eq. (8), if the pulse energy of 4.67 mJ is divided by the pulse duration of 0.15 ms, a pulse power of 31 W is obtained.

In the article of Muhammad et al. [21], the examination of the ideal laser cutting setting can be done by following the steps described in Kleine et al. [19] leads to an average power of 20 W and a pulse energy of 10.00 mJ.

Repeating the calculations described in the analysis of the Meng et al. [20], the pulse energy and pulse power from the articles by Chen et al. [8], Chen et al. [22] and Catalano et al. [11] can be obtained, which are shown in Table 8 [8, 11, 19–22].

Analyzing, line by line, the calculated missing data for fiber laser stent fabrication, given in italics in Table 8 [8, 11, 19–22]: by rearranging Eq. (7) for DBT, the cutting speed divided by the frequency, it gives the

distance between two pulses in  $\mu\text{m}$ . From Eq. (13), the spot overlap can be calculated for all six machining operations listed in rows 10 and 11 of Table 8 [8, 11, 19–22].

Based on the focal spot diameter, which is given in all articles, the energy per unit volume can be calculated from Eq. (9). The energy per unit volume can be calculated from Eq. (10) based on the width of the kerf cross-section, which is given only in the first four articles, and is listed in rows 14 and 15 of Table 8 [8, 11, 19–22].

Comparing the reported and calculated data of the 6 analyzed publications, the following conclusions can be drawn:

- Kleine et al. [19] were able to cut a stent with the lowest average performance.
- Catalano et al. [11] cut by ablation, i.e., vaporization, because of the very short pulse duration, and needed a high spot overlap: 99.65%, and therefore had the lowest cutting speed: 2 mm/s.
- Chen et al. [8] were able to cut the fastest at 20 mm/s, which is higher than the 15 mm/s achieved in our own experiment due to the small focal spot size resulting from the superior beam quality of the fiber laser and due to the second highest repetition rate of 15 kHz. Here, a cut spot overlap of around 89% was enough to make the cut.

**Table 8** Calculated missing data for fiber laser stent manufacturing\*

	Unit of measurement	Kleine et al. [19]	Meng et al. [20]	Muhammad et al. [21]	Chen et al. [8]	Chen et al. [22]	Catalano et al. [11]
Material		316L	316L	316L	316LVM	316LVM	316L
Wall thickness	$\mu\text{m}$	100	110	150	80	100	200
Average power	W	<i>1.5</i>	7.0	<i>20.0</i>	5.8	5.8	11
Pulse time	ms	0.1	0.15	0.1	0.07	0.007	0.00025
Pulse energy	mJ	<i>3.00</i>	<i>4.67</i>	<i>10.00</i>	<i>0.39</i>	<i>3.87</i>	<i>0.44</i>
Pulse power	W	30	31	100	6	552	1760
Pulse frequency	Hz	500	1500	2000	15000	1500	25000
Cutting speed	mm/s	4	8	16.7	20	12	2
Distance between two pulses on material	$\mu\text{m}$	<i>8.00</i>	<i>5.33</i>	<i>8.33</i>	<i>1.33</i>	<i>8.00</i>	<i>0.08</i>
Focal spot diameter	$\mu\text{m}$	16.00	12.00	25.00	12.00	12.00	23
Spot overlap	%	<i>50.00</i>	<i>55.56</i>	<i>66.67</i>	<i>88.89</i>	<i>33.33</i>	<i>99.65</i>
Top kerf's cross-section width	$\mu\text{m}$	19	20	30	20	–	–
Energy per unit volume based on focal spot diameter	J/mm <sup>3</sup>	<i>234</i>	<i>663</i>	<i>320</i>	<i>302</i>	<i>403</i>	<i>1196</i>
Energy per unit volume based on the cross-sectional width of the kerf	J/mm <sup>3</sup>	<i>197</i>	<i>398</i>	<i>267</i>	181	–	–
$Z_R$	$\mu\text{m}$	<i>160</i>	–	–	96	–	230

\* The calculated data are in italics

### 7 Analysis of articles on ultrafast lasers using ps and fs pulses

The analysis of the calculated missing data for stent manufacturing lasers using ultrashort laser pulses, given in italics in Table 9 [1, 11, 14]. Here, only  $Z_R$ s have been calculated from 3 publications [1, 11, 14], but analysis of the other data may be also useful. The Trumpf TruMicro 5350 laser used in Muhammad's PhD thesis [1] has the smallest focal spot diameter due to its wavelength being one third of that of a conventional fiber or Nd:YAG laser, and it follows from Eq. (1) that the spot diameter decreases linearly with decreasing wavelength. The ultrashort pulse time implies that the machining is done by ablation, i.e., a small layer is evaporated by the laser on the cutting line, so the cutting line has to be passed several times with the laser. Pulse times vary from 250 ns to 100 fs. In Table 10 [1, 11, 14] the analysis of the machine data can be seen, it is about the articles that had data for this, so the articles are slightly different from those in Table 9 [1, 11, 14]. Table 10 [1, 11, 14] shows that for the 6 ps pulses, the cutting line had to be passed 3 times, while for the shortest 100 fs pulses, it had to be passed up to 297 times. At 6 ps pulses, dross-free cutting could be achieved at the cost of low cutting speeds in the range 0.42–2 mm/s.

In Table 10, the data calculated here that are missing from the publications are shown in italics and are obtained in the same way as previously described. Muhammad's PhD thesis [1] examines the effect of water being led across the tube workpiece during laser cutting of a stent: the cooling water causes the cutting speed to be low, but the slag does not stick to the bottom of the cut or the opposite tube wall, so minimal post-processing is required. It is also interesting to note that ablation requires a lot of low-energy pulses to cut through the material, which is

only possible with higher pulse frequencies than before: values of 1–200 kHz. The cut spot overlap is above 98% everywhere, the distance between two pulses on the material is around 1 nm in Muhammad's PhD thesis [1], see the first column of Table 10.

### 8 Cut quality evaluation and product safety for stent production by laser

In Meszlényi et al. [23], the analysis of the laser cut cross-section of 304L tubes cut in axial direction was made, which illustrates many cutting errors due to the early experiment.

By analyzing the cross-section of the kerf (Figs. 7 and 8), the following cutting errors can be seen:

- A conical kerf cross-section described by a taper angle Eq. (14):

$$a = \tan^{-1} \left( \frac{k_1 - k_2}{2a_v} \right), \tag{14}$$

where  $a$  is the taper angle,  $k_1$  is the upper width of the kerf cross-section,  $k_2$  is the lower width of the kerf cross-section,  $a_v$  is the wall thickness. The oxide layer is a black layer on the outer edge of the cutting gap cross-section due to accelerated cutting with oxygen as the cutting gas.

- Reflowed layer, which is a layer of molten and then re-solidified metal in the cross-section of the kerf.
- Heat-affected zone: following the reflowed layer, this is in fact the metal layer that has been heat-treated by the laser.
- Adhesive slag: slag is produced by cutting accelerated with oxygen, and some of it sticks to the bottom of the kerf (Fig. 8), while some of it splashes and sticks to the opposite internal wall of the tube.

**Table 9** Beam characteristics of the ultra-short pulse lasers used by stent manufacturers\*

Author and publication	Muhammad [1]	Muhammad [1]	Demir and Previtali [14]	Demir and Previtali [14]	Catalano et al. [11]
Laser system	Trumpf TruMicro 5350	Coherent Libra Ti: Sapphire	IPG YLP-1/100/50/50 Q-coupled fiber laser	Rofin StarFemto, Fiber optic	IPG YLP-1/100/50/50 Q-coupled fiber laser
$d_{f0}$ (μm)	5.2	100	23	32	23
$f$ (mm)	–	100	50	50	60
Wavelength (μm)	0.343	0.8	1.064	1.552	1.064
$M^2$	1.2	–	1.7	1.3	1.7
$d_b$ (mm)	–	6	5.9	4	–
$Z_R$ (μm)	–	<i>1667</i>	<i>195</i>	<i>400</i>	–
Pulse time given in article	6 ps	100 fs	250 ns	800 fs	250 ns
Pulse time converted to ms	6.00E–09	1.00E–10	2.50E–04	8.00E–10	2.50E–04

\* The calculated data are in italics

**Table 10** Completed stent cutting parameters for ultrashort pulse lasers\*

Cutting parameters	Unit	Author and publication				
		Muhammad [1]	Muhammad [1]	Muhammad [1]	Demir and Previtali [14]	Catalano et al. [11]
		Laser system				
		Trumpf TruMicro 5350	Coherent Libra Ti: Sapphire	IPG YLP-1/100/50/50fiber Q coupled	Material	
		Nitinol	Pt-Cr alloyed steel	Nitinol	AZ31 Mg-alloy	316L
Wall thickness	μm	280	67	180	200	200
Average power	W	10	7	<i>1</i>	7,5	11
Pulse time	ms	6.00E-09	6.00E-09	1.00E-10	2.50E-04	2.50E-04
Pulse energy	mJ	<i>0.05</i>	<i>0.04</i>	<i>1</i>	0.3	0.44
Pulse power	W	<i>8.33E+06</i>	<i>5.83E+06</i>	<i>1.00E+10</i>	<i>1.20E+03</i>	<i>1760.00</i>
Pulse frequency	Hz	200000	200000	1000	25000	25000
Cutting speed	mm/s	0.42	1.67	1.5	2	2
Distance between two pulses on material	μm	<i>2.10E-03</i>	<i>8.35E-03</i>	<i>1.50E+00</i>	<i>8.00E-02</i>	<i>0.08</i>
Focal spot diameter	μm	5.2	5.2	100	23	23
Spot overlap	%	<i>99.96</i>	<i>99.84</i>	<i>98.50</i>	<i>99.65</i>	<i>99.65</i>
Energy per unit volume based on focal spot diameter	J/mm <sup>3</sup>	<i>1.64E+04</i>	<i>1.20E+04</i>	<i>3.70E+01</i>	<i>8.15E+02</i>	<i>1.20E+03</i>
$Z_R$	μm	–	–	1667	195	230
How many times to cross the cut line	–	3	3	15–297	–	–
Quality of laser cut	–	Dross-free	Dross-free	–	–	–

\* Calculated missing data are seen in italics

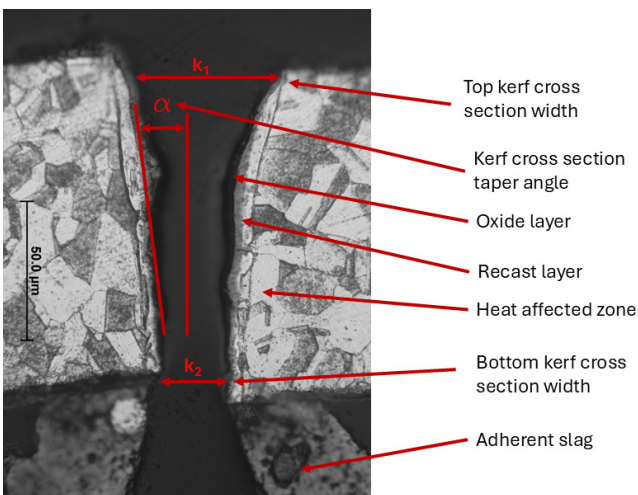


**Fig. 7** Cross-section of the kerf after the laser cut of 1.200 mm diameter, 0.120 mm wall thickness tube of AISI 304L type stainless steel

- Micro cracks in the material, this are not observed here.
- The surface roughness ("ribbing") of the cut surface, which is removed during finishing and is difficult to measure: an optical roughness tester is needed, usually indicated in publications as  $R_{max}$ .

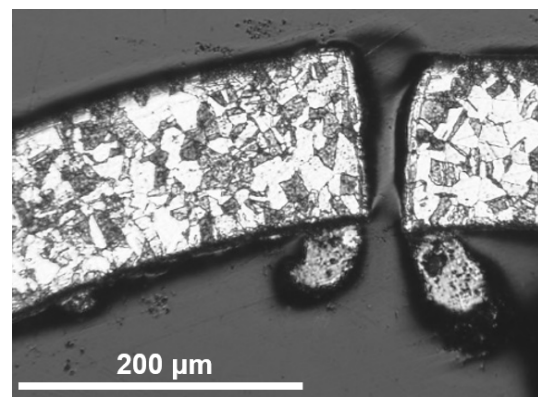


**Fig. 8** Adherent slag on the inside of the tube;  $D = 1.200$  mm,  $s = 0.120$  mm, material: AISI 304L steel. The cutting was performed by using Corina stent cutting system developed in Hungary

The relationships between the technological parameters of laser stent cutting are described in Eqs. (1) to (14), and the inter-calculability of each parameter is shown in Fig. 9. In doing so, a new method has been developed that allows and illustrates the computability of the entire parameter system.

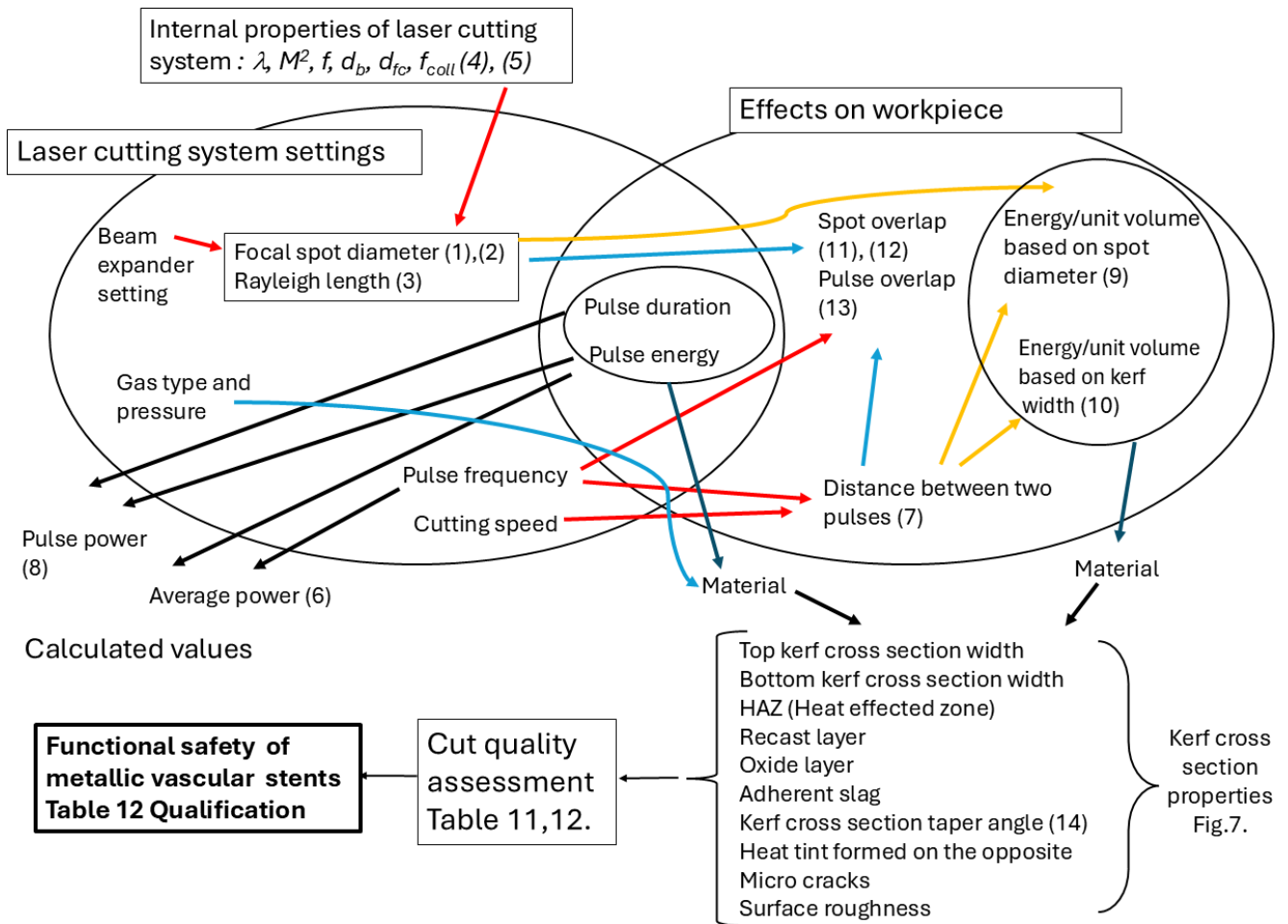


Fig. 9 Correlation of laser cutting parameters with functional safety of stents. The numbers of the equations in this article are in parentheses in this figure, further explanation can be found in the text

Besides the parameters in internal properties of laser cutting the missing values can be calculated using Eqs. (4) and (5). Adding Beam expander setting to this parameter group focal spot diameter and ZR can be computed using Eqs. (1) to 3. From pulse energy and pulse frequency the average power can be obtained with the aid of Eq. (6). Using pulse frequency and cutting speed the distance between two pulses can be received (Eq. (7)). From pulse energy and pulse frequency the pulse power can be reckoned with the aid of Eq. (8). From focal spot diameter and distance between two pulses the energy/unit volume based on spot diameter (Eq. (9)) can be calculated. Using kerf width and distance between two pulses the energy/unit volume based on kerf width can be obtained (Eq. (10)). Based on Eqs. (11) and (12) the spot overlap, based on Eq. (13) the pulse overlap can be calculated. The taper angle of conical kerf cross-section can be computed using Eq. (14).

The laser cutting parameters and its effects on workpiece have an influence on the kerf cross-section, which

is the base of cut quality assessment leads to the qualification of the cut.

Finally, a ranking system was developed to quantify the laser stent cutting errors and multiply them by a weight factor to calculate the cut quality; the ranking system is presented in Table 11. In Table 11, the dimensionless parameters based on size are based on the magnitude of the laser cutting error, divided by a reference value. For the weight factors, a lower value of weight was used for defects that could be removed in post-machining, and a higher value for those that remained.

Post-processing can be etching and electro polishing. In evaluating the amount of cut error, the set of minimum-acceptable limit is done, so that the kerf cross-section illustrated in Figs. 7 and 8 meets it. The heat damage on the cut opposite side of the laser-machined tube is shown in Fig. 10, where no heat damage is observed at the cut settings of the left tube.

**Table 11** Evaluation system for stent cutting imperfections

Parameter	Dimension-based dimensionless parameter	Weight factor	Justification
Heat affected zone	Width/10 $\mu\text{m}$	0.5	
Refused layer	Width/5 $\mu\text{m}$	0.5	Can be removed with post processing, but takes time
Oxide layer	Width/5 $\mu\text{m}$	0.5	
Adherent slag	Slag height/20 $\mu\text{m}$	0.5	Remains intact despite post processing, it just rounds off
Kerf cross-section taper angle	Taper angle/ $5^\circ$	2	
Micro cracks	Depth/2 $\mu\text{m}$	0.5	Can be removed by post processing, but takes time
Surface roughness	$R_{\text{max}}/2 \mu\text{m}$ estimable	0.1	
Upper width of the kerf cross-section	Width/20 $\mu\text{m}$	1	A lot of melted material causes a lot of slag and a lot of splashing, although it can be removed by post processing
Bottom width of the kerf cross-section	Width/20 $\mu\text{m}$	0.5	
Heat effect at the opposite inner side of the tube	Width/10 $\mu\text{m}$	3	Not allowed
			0–3 excellent
			4–6 good
			7–10 acceptable
			11 to not acceptable
Kerf error sum	To be added up, to be rated on this basis		

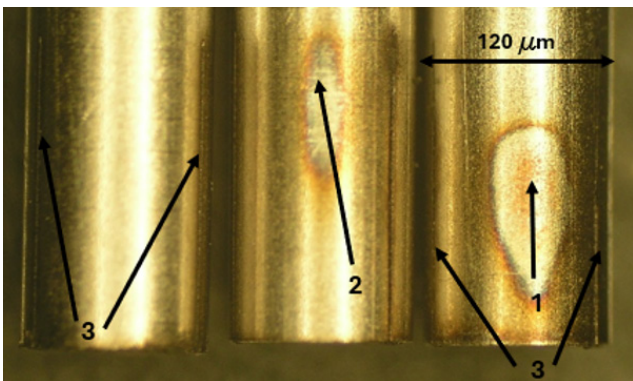


**Fig. 10** Heat tint formed on the opposite external surface of the laser-cut tube; 1: Strong heat tint, 2: Weak heat tint, 3: Another cut line

Finally, Table 12 shows a cut quality evaluation, based on Fig. 7 and Fig. 8, which was performed using the JMicroVison image analysis software for serial measurements. The assessment is based on Table 11. The result of the evaluation is a truncation error amount of 9.03, which is just acceptable. In this way, I have developed an evaluation system to determine how factors affect the quality and safety of the stent product. The point is that even if the laser cut stent does show cutting defects, the post-processing should remove or reduce them to the stage where the stent implanted in the human body does not cause problems. In almost all publications on laser stent cutting, oxygen has been used as a working gas to accelerate cutting, but there is an oxide layer, a refused layer, a heat-affected zone, a slag. The rib size of the stent must be determined in such a way that the correct size is obtained after

post-processing. If the kerf can be reduced by reducing the energy per unit volume, the amount of slag and slag splashing is reduced, so less post-processing is needed.

### 9 Conclusion

Publications on fiber laser systems for producing vascular stents often do not provide all the technological variables needed to determine the important parameters of the focused beam's cross-section, the focal spot diameter and the ZR. Here is a method presented to determine the missing data of stent fiber lasers in scientific publications, using a combination of formulas found in different places in the literature.

The setup parameters for laser cutting with a pulsed laser are not independent of each other, which gives the possibility to calculate some missing data of articles: this way, data from different articles can be better compared and experiments can be repeated, which is a useful basis for further development of a technology. For this purpose, a new method was developed that allows the determination and calculation of the entire parameter system required for laser stent cutting. The correlation of laser cutting parameters with the functional safety for stents was elaborated.

The distance between two pulses (DBT) defined: the distance between the centers of two successive pulses hitting the workpiece. Also presented two formulas calculating the energy per unit volume based on the focal spot diameter and based on width of the top kerf cross-section width.

Finally, a ranking system was developed to quantify the laser stent cutting errors and multiply them by a weight

**Table 12** Cut quality assessment

Parameter	Dimension based dimensionless parameter	Weight factor	Measured value 1	Measured value 2	Measured value 3	Average of measured values	Meter number
Heat affected zone	Width/10 μm	0.5	3.2	2.5	3.2	3.0	0.30
Refused layer	Width/5 μm	0.5	5.4	3.4	5.5	4.8	0.48
Oxide layer	Width/5 μm	0.5	2.3	2.9	2.5	2.6	0.26
Adherent slag	Slag height/20 μm	0.5	61	44	55	53.3	1.33
Kerf cross-section taper angle	Taper angle <sup>o</sup> / 5°	2	10	6	8	8	3.20
Micro cracks	Depth/2 μm	0.5	0	0	0	0	0
Surface roughness	$R_{max}/2$ μm estimable	0.1	4	5	3	4	0.20
Upper width of the kerf cross-section	Width/20 μm	1	59	48	52	53	2.65
Bottom width of the kerf cross-section	Width/20 μm	0.5	24	26	24	24.67	0.62
Heat effect at the opposite inner side of the tube	Width/10 μm	3	0	0	0	0	0
Kerf error sum	To be added up, to be rated on this basis	–	–	–	–	–	9.03
						Qualification	Acceptable

factor to calculate the cut quality; the ranking system is presented in Table 11. In Table 11, the dimensionless parameters based on size are based on the magnitude of the laser cutting error, divided by a reference value. For the weight

factors, a lower value of weight was used for defects that could be removed in post-machining, and a higher value for those that remained. This gives a cut quality evaluation and product safety for stent production by laser.

**References**

[1] Muhammad, N. "Laser Micromachining of Coronary Stents for Medical Applications", PhD Thesis, The University of Manchester, 2012. [online] Available at: <https://research.manchester.ac.uk/en/studentTheses/laser-micromachining-of-coronary-stents-for-medical-applications> [Accessed: 14 November 2024]

[2] Kaplan, A. "Theoretical Analysis of Laser Beam Cutting", Shaker Verlag, 2002. ISBN 3-8322-0803-8

[3] Harp, W. R., Paleocrassas, A. G., Tu, J. F. "A Practical method for determining the beam profile near the focal spot", The International Journal of Advanced Manufacturing Technology, 37(11), pp. 1113–1119, 2008. <https://doi.org/10.1007/s00170-007-1067-z>

[4] Meszlényi, G., Bitay, E. "Analysis of Fibre Laser's Optical Construction from the End of the Beam Guiding Optical Fibre to the Focal Spot", Acta Materialia Transylvanica, 5(2), pp. 72–77, 2022. <https://doi.org/10.33924/amt-2022-02-05>

[5] ISO "ISO 11146-1:2021 Lasers and laser-related equipment — Test methods for laser beam widths, divergence angles and beam propagation ratios: Part 1: Stigmatic and simple astigmatic beams", International Organization for Standardization, Geneva, Switzerland, 2021.

[6] Sill Optics "Technical Guide: Laser Optics – Formulary", [online] Available at: <https://www.silloptics.de/en/service/sill-technical-guide/laser-optics/formelsammlung> [Accessed: 14 November 2024]

[7] Mendes, M., Sarrafi, R., Schoenly, J., VanGemert, R. "Fiber laser micromachining in high-volume manufacturing", Industrial Laser Solutions, May 11., 2015. [online] Available at: <https://www.laserfocusworld.com/industrial-laser-solutions/article/14216389/fiber-laser-micromachining-in-high-volume-manufacturing> [Accessed: 14 November 2024]

[8] Chen, C.-S., Lin, S.-Y., Chou, N.-K., Chen, Y.-S., Ma, S.-F. "Optimization of Laser Processing in the Fabrication of Stents", Materials Transactions, 53(11), pp. 2023–2027, 2012. <https://doi.org/10.2320/matertrans.M2012188>

[9] Demir, A. G., Previtali, B., Biffi, C. A. "Fibre Laser Cutting and Chemical Etching of AZ31 for Manufacturing Biodegradable Stents", Advances in Materials Science and Engineering, 2013(1), 692635, 2013. <https://doi.org/10.1155/2013/692635>

[10] García-López, E., Medrano-Tellez, A., Ibarra-Medina, J., Siller, H. R., Elías-Zúñiga, A., Ciro, A. R. "Fiber Laser microcutting of AISI 316L stainless steel tubes- influence of pulse energy and spot overlap on back wall dross", Procedia CIRP, 49, pp. 222–226, 2016. <https://doi.org/10.1016/j.procir.2015.11.020>

[11] Catalano, G., Demir, A. G., Furlan, V., Previtali, B. "Use of Sheet Material for Rapid Prototyping of Cardiovascular Stents", Procedia Engineering, 183, pp. 194–199, 2017. <https://doi.org/10.1016/j.proeng.2017.04.019>

- [12] Thawari, G., Sundar, J. K. S., Sundararajan, G., Joshi, S. V. "Influence of process parameters during pulsed Nd:YAG laser cutting of nickel-base superalloys", *Journal of Materials Processing Technology*, 170(1–2), pp. 229–239, 2005.  
<https://doi.org/10.1016/j.jmatprotec.2005.05.021>
- [13] Meszlényi, G., Izápy, V. "Optimization Method of Laser Cutting Parameters for High Precision Stainless Steel Tubes", In: 26th International Conference Science in Practice (SiP 2008), Osijek, Croatia, 2008, pp. 95–98. ISBN 978-953-6032-62-4
- [14] Demir, A. G., Previtali, B. "Comparative study of CW, nanosecond- and femtosecond-pulsed laser microcutting of AZ31 magnesium alloy stents", *Biointerphases*, 9(2), 029004, 2014.  
<https://doi.org/10.1116/1.4866589>
- [15] Kathuria, Y. P. "Laser microprocessing of metallic stent for medical therapy", *Journal of Materials Processing Technology*, 170(3), pp. 545–550, 2005.  
<https://doi.org/10.1016/j.jmatprotec.2005.05.041>
- [16] Meszlényi, G., Bitay, E. "Role of the Features of Focused Laser Beam at Pulsed Laser Cutting", *Acta Materialia Transylvanica*, 2(2), pp. 115–120, 2019.  
<https://doi.org/10.33924/amt-2019-02-09>
- [17] Bitay, E., Puskás, Z., Kulin, T., Meszlényi, G., Dobránszky, J. "Bioanyagok lézersugaras vágási technológiája" (Laser cutting technology of biomaterials), In: 27. Hegesztési Konferencia, Budapest, Hungary, 2014, pp. 405–414. ISBN 978-963-08-8585-0 (in Hungarian) [online] Available at: <http://real.mtak.hu/id/eprint/21187> [Accessed: 14 November 2024]
- [18] Nagy, P., Dobránszky, J. "Laser Cutting of Small Diameter Nitinol Tube", *Materials Science Forum*, 729, pp. 460–463, 2012.  
<https://doi.org/10.4028/www.scientific.net/MSF.729.460>
- [19] Kleine, K. F., Whitney, B., Watkins, K. G. "Use of fiber lasers for micro cutting applications in the medical device industry", In: ICALEO 2002: 21st International Congress on Laser Materials Processing and Laser Microfabrication, Scottsdale, AZ, USA, 2002, pp. 1–11. ISBN 978-0-912035-72-7  
<https://doi.org/10.2351/1.5065757>
- [20] Meng, H., Liao, J., Zhou, Y., Zhang, Q. "Laser micro-processing of cardiovascular stent with fiber laser cutting system", *Optics & Laser Technology*, 41(3), pp. 300–302, 2009.  
<https://doi.org/10.1016/j.optlastec.2008.06.001>
- [21] Muhammad, N., Whitehead, D., Boor, A., Li, L. "Comparison of dry and wet fibre laser profile cutting of thin 316L stainless steel tubes for medical device applications", *Journal of Materials Processing Technology*, 210(15), pp. 2261–2267, 2010.  
<https://doi.org/10.1016/j.jmatprotec.2010.08.015>
- [22] Chen, C. S., Lin, S. Y., Chou, N. K. "Optimization Technology and Developing of Vascular Stents", *Applied Mechanics and Materials*, 284–287, pp. 390–397, 2013.  
<https://doi.org/10.4028/www.scientific.net/AMM.284-287.390>
- [23] Meszlényi, G., Dobránszky, J., Puskás, Z. "Laser Cutting of High Precision Tubes", *Materials Science Forum*, 589, pp. 427–431.  
<https://doi.org/10.4028/www.scientific.net/MSF.589.427>